Electronic Supplementary Material (ESI) for ChemComm.

Synthesis ammonia via electrochemical nitrogen reduction on high-index faceted Au nanoparticles with a high Faradaic efficiency

Lianqiao Tan,[a] Na Yang,[a] Xun Huang,*[a] Lishan Peng,[a] Cheng Tong,[a] Mingming Deng,[a] Xianyi Tang,[a] Li Li,[a] Qiang Liao,[b, c] Zidong Wei*[a]

a National-municipal Joint Engineering Laboratory for Chemical Process Intensification and Reaction, College of Chemistry and Chemical Engineering, Chongqing University, Chongqing, 400044, China

b Key Laboratory of Low-grade Energy Utilization Technologies and Systems, Ministry of Education, Chongqing 400030, China

c Institute of Engineering Thermophysics, School of Energy and Power Engineering, Chongqing University, Chongqing 400030, China

*E-Mail: zdwei@cqu.edu.cn; huangxun@cqu.edu.cn

Experimental Section

Materials: Hexadecyl trimethyl ammonium bromide (CTAB), hexadecyl trimethyl ammonium chloride (CTAC), sodium bromide (NaBr), ascorbic acid (AA), L-cysteine, salicylic acid, sodium hydroxide, sodium citrate, sodium hypochlorite (NaClO), sodium nitroprusside, para-(dimethylamino) benzaldehyde (p-$C_9H_{11}NO$), hydrochloric acid (HCl), ethanol were purchased from Chuandong Chemical Group Co., Ltd., Chloroauric acid ($HAuCl_4$) was purchased from Aladdin Ltd. (Shanghai, China). Diluted water throughout all experiments was purified through a Millipore system.

Synthesis of rhombic dodecahedra gold seeds and AuNPs: Rhombic dodecahedra gold seeds were prepared according to Huang.[1] Typically, a volume of 1 mL of 2.5 mM $HAuCl_4$ solution was dropped into 9 mL aqueous solution containing 1 mmol CTAC under vigorous stirring. To the mixture was injected 0.45 mL of 0.02 M ice-cold $NaBH_4$ solution under stirring for another 5 min. The obtained gold seeds solution was kept for 2 h at 4 ^oC. For the synthesis of rhombic dodecahedra gold seeds, growth solution containing 100 mM CTAC, 0.25 mM $HAuCl_4$, 0.01 mM NaBr and 0.6 mM AA was prepared. Under stirring, 25 μL as-prepared gold seeds solution was injected into 10 mL growth solution for 5s, then 250 μL of the mixture was transferred into 100 mL of the growth solution with thorough mixing for 20s. The solution was left disturbed for 20 min for gold nanoparticle incubation and centrifuged at 6000 rpm for 5 min. After washed by diluted water, the obtained rhombic dodecahedra gold seeds were dispersed in 1 mM CTAB solution.

For synthesis of AuNPs, a growth solution was prepared by mixing 16 mL of 0.1 M

CTAB and 400 µL of 0.1 M ($HAuCl_4$) solution in 79 mL of diluted water under vigorous stirring. After rapid injection of 9.5 mL of 0.1 M ascorbic acid (AA) solution, 100 µL of 2 mM L-cysteine solution was added into the growth solution.[2] Finally, the as-prepared octahedral seeds in CTAB solution were introduced. After incubation for 2 h, AuNFs were obtained by concentration and washed twice, and then re-dispersed in 0.1 mM CTAC solution with mass concentration of 10 mg mL^{-1} for further use.

Characterization: Scanning electron microscopy (SEM) measurements were conducted on JSM-7800F (JEOL) field emission scanning electron microscope operated at 15 kV. Transmission electron microscopy (TEM) and high-angle annular dark-field scanning transmission electron microscope (HAADF-STEM) was carried out on a Talos F200S G1 instrument operating at 200 kV. The UV-vis spectra were obtained from UV-vis-NIR spectroscopy (TU1806, Beijing Purkinje General).

Electrode Preparation: 10 µL of Au nanoparticles suspension (10 mg mL^{-1}) was dropped onto the 0.5 cm × 0.5 cm carbon paper and dried in a vacuum at 30℃ for 5 h. The obtained carbon paper electrode deposited with catalyst was immersed into ethanol several times to remove the remaining CTAC, and used a working electrode.

Electrochemical Methods: All the electrochemical NRR measurements were performed in a 0.1 M Li_2SO_4 solution in a typical three-electrode system using a CHI instrument potentiostat (CHI, 660E). The graphite plate and a silver/silver chloride electrode (Ag/AgCl; saturated KCl electrolyte) were employed as counter electrode and reference electrode, respectively. In this work, all applied potentials were iR-compensated and converted to the RHE scale using the following equation:

$E_{(RHE)} = E_{(Ag/AgCl)} + (0.197 + 0.059 \times pH)V$

Prior to electrolysis, high-purity N_2 (99.999%) or Ar (99.999%) was continuously purged into 0.1 M Li_2SO_4 solution for at least 30 min. LSV measurements were performed in a voltage window from -0.8 V to +0.1 V vs. RHE at scan rates of 1 mV s^{-1}. All LSV curves were steady state after several cycles. Potentiostatic tests were conducted at different potentials (-0.1, -0.2, -0.3, -0.4, -0.5 V vs. RHE) in 0.1 M Li_2SO_4 solution (30 mL) bubbled with a continuous N_2 flow for 2 h. The current densities were normalized to the geometrical areas.

Determination of NH_3 via indophenol blue method and ion chromatography method: The concentration of ammonia produced was detected via indophenol blue method using UV-vis-NIR spectroscopy.[3] Typically, 2 mL electrolyte was removed from the cathode chamber and mixed with 2 mL of 1 M NaOH solution containing 5 wt% salicylic acid and 5 wt% sodium citrate, followed by the addition of 1 mL of NaClO solution and 200 μL of 1 wt% sodium nitroferricyanide solution. After incubation at room temperature for 2 h, the UV-vis adsorption spectra with absorbance at 655 nm was measured using a spectrophotometer. For accurate NH_3 quantification, the calibration curve was plotted by employing ammonium chloride standard solutions.

The quantity of NH_3 formation was also measured by ion chromatograph (ICS-1100, Thermo Dionex), equipped with electrical conductivity detector, autosampler, protective column and analysis column (CG12 (2*50mm)) and analysis column (CS12(4*250mm)). The eluent was methyl sulfonic acid solution (20 mM), and the flow velocity was 1.21 mL min^{-1}. The suppressor current was 71 mA. The column

temperature was 31℃. The peaks of NH_4^+ and K^+ are at 4.13 min and 5.08 min, respectively. Before analysis, the electrolytic solutions were diluted 10 times with deionized water.

Determination of N_2H_4: The method of Watt and Chrisp was employed to quantify he amount of hydrazine formation after electrolysis.[4] Typically, color reagent containing p-$C_9H_{11}NO$ (5.99 g), HCl (concentrated, 30 mL), ethanol (300 mL) was pre-prepared. 2 mL of electrolyte after NRR tests was transferred into 2 mL the color reagent and kept for 15 min at room temperature. The absorption spectra of resulting solution were measured at 455 nm. To obtain the calibration curve, a series of 0.1 M Li_2SO_4 solution containing hydrazine with known concentration were used as calibration standards.

Calculations of NH_3 yield and Faradaic efficiency:

The NH_3 yield is estimated using the following equation:

$$NH_3 \text{ yield } \left(\mu g\ h^{-1}\ cm^{-2}\right) = \frac{c_{NH_3} \times V}{A \times t}$$

The ammonia Faradaic efficiency is calculated according to the following equation:

$$FE_{NH_3}(\%) = \frac{3 \times F \times c_{NH_3} \times V}{Q} \times 100\%$$

Where c_{NH_3} is the ammonia concentration (μg mL^{-1}), V is the volume of the electrolyte (30 mL), A is the geometric area of the working electrode, t is the electrolysis time, F is the Faraday constant, Q is the quantity of the applied electricity.

Isotope-labelled experiments: Isotope labeling test was conducted to identify the source of ammonia using $^{15}N_2$ as feeding gas. After electrolysis, the $^{15}NH_4^+$ production was collected by HCl solution, and then dried with vacuum evaporator. The sample

collected was redispersed using D_2O and detected via ^{1}H-NMR measurements (Bruker NMR400, 400MHz). The ^{1}H-NMR signal of ^{15}N produces a double coupling (~72 Hz) at the chemical shift of ~7 ppm.

DFT method: Our computational simulations were performed by Vienna ab-initio simulation package (VASP) with the projector augmented wave pseudo-potentials (PAW) to describe the interaction between atomic cores and valence electrons with density functional theory (DFT). The Perdew–Burke–Ernzerhof (PBE) functional within the generalized gradient approximation (GGA) were used to implement DFT calculations.[1] Four layered Au (110), Au(553) and five layered Au(551) slab models were employed to simulate the catalyst surface. In all of the structure optimization calculations, the bottom two layers of Au(551), and three layers of Au(110) and Au(553) were fixed, while the other atoms were fully relaxed. The reasonable vacuum layers were set around 15 Å in the z-directions for avoiding interaction between planes. A cutoff energy of 400 eV was provided and a 3×2×1 Monkhorst Pack k-point sampling was chosen for the well converged energy values. Geometry optimizations were pursued until the force on each atom falls below the convergence criterion of 0.02 eV/Å and energies were converged within 10^{-5} eV. The change of Gibbs free energy (ΔG) for each elemental step can be computed by:

$$\Delta G = \Delta E + \Delta ZPE - T\Delta S + \Delta G_U + \Delta G_{pH}$$

where ΔE and ΔZPE are the electronic energy difference and the change in zero-point energies, respectively, which are directly obtained from DFT calculations. T is the temperature (T = 298.15 K in this work). ΔS is the entropy change. ΔG_U=-neU (n and U

are the number of transferred electrons and the electrode potential applied, respectively). ΔG_{pH} is the contribution of H^+, which can be determined as $\Delta G_{pH} = 2.303 \times kBT \times pH$, where k_B is the Boltzmann constant.

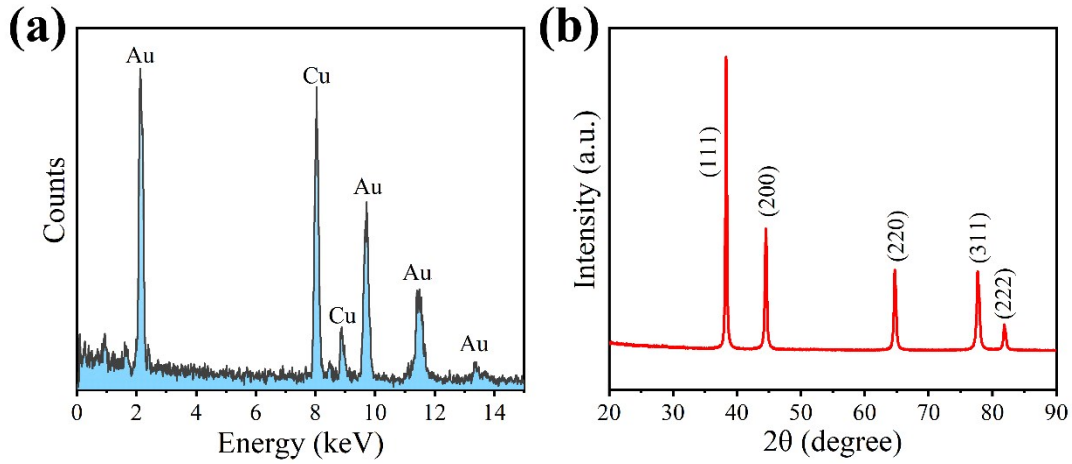

Figure S1. (a) TEM-EDS and (b) XRD patterns of AuNPs.

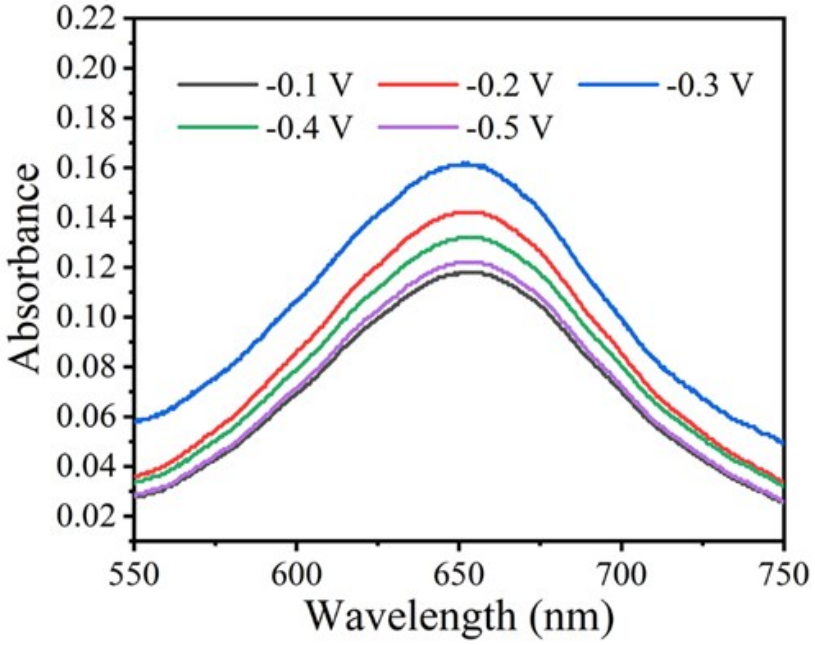

Figure S2. UV-vis absorption spectra of the electrolytes stained with indophenol indicator for AuNPs at different applied potentials in N_2-saturated 0.1 M Li_2SO_4 solution at 20℃.

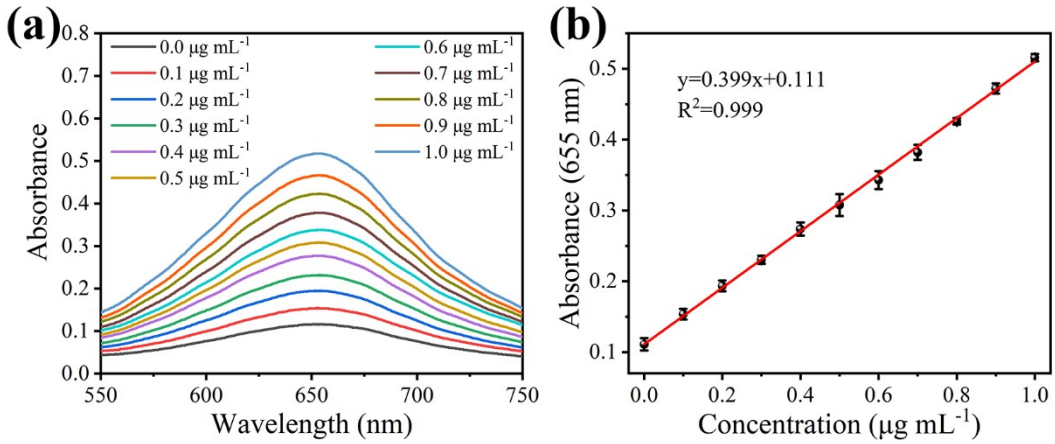

Figure S3. Quantification of ammonia via indophenol blue method. (a) UV-vis absorption spectra and (b) calibration curves for ammonia assay via Salicylic acid spectrophotometry. Error bars in (b) correspond to the standard deviations of three independent measurements.

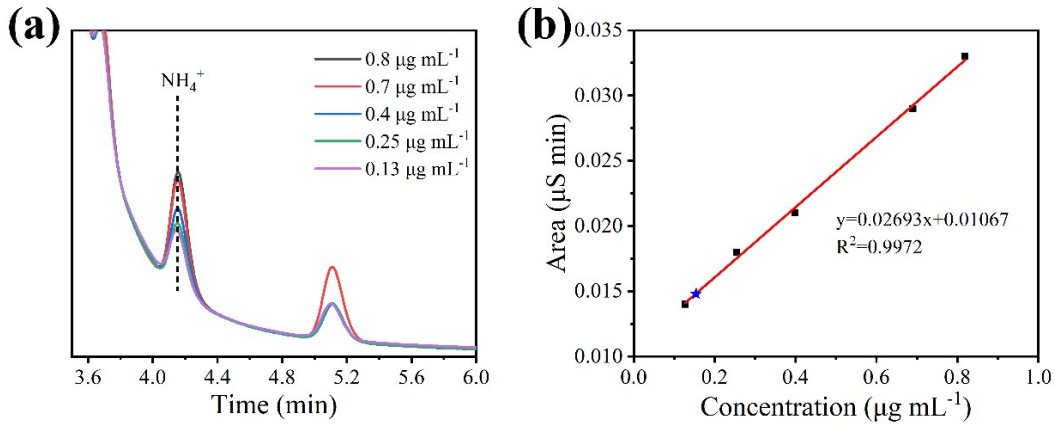

Figure S4. Quantification of ammonia via ion chromatography method. (a) Ion chromatography f of standard NH^4+ samples with various concentrations. (b) Calibration curve of peak area for standard solutions of NH_4^+ and NRR sample. The black squares represent the concentrations and IC peak area values for the standard samples. The blue star shows the concentration of NH4+ in the electrolytes after electrolysis at –0.3 V vs RHE for 2 hours.

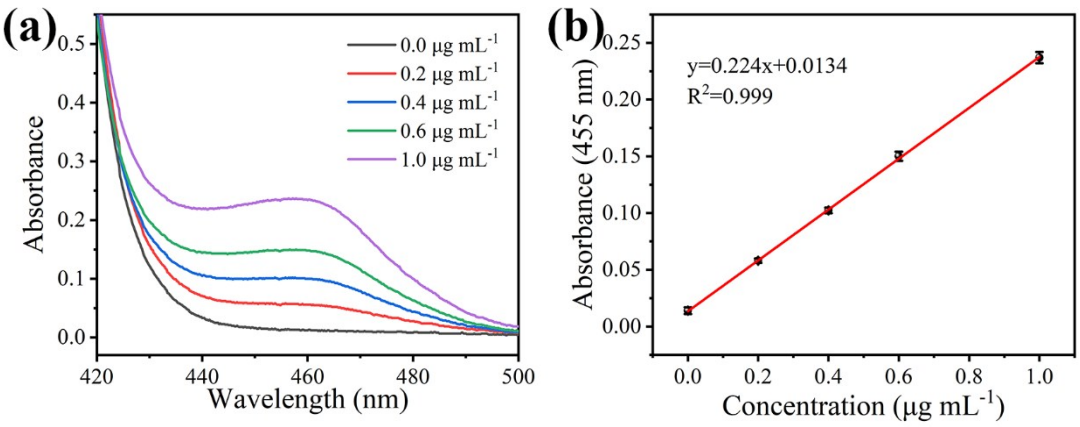

Figure S5. Quantification of hydrazine. (a) UV-vis absorption spectra and b) calibration curves for hydrazine assay via Watt and Chrisp's method. Error bars in (b) correspond to the standard deviations of three independent measurements.

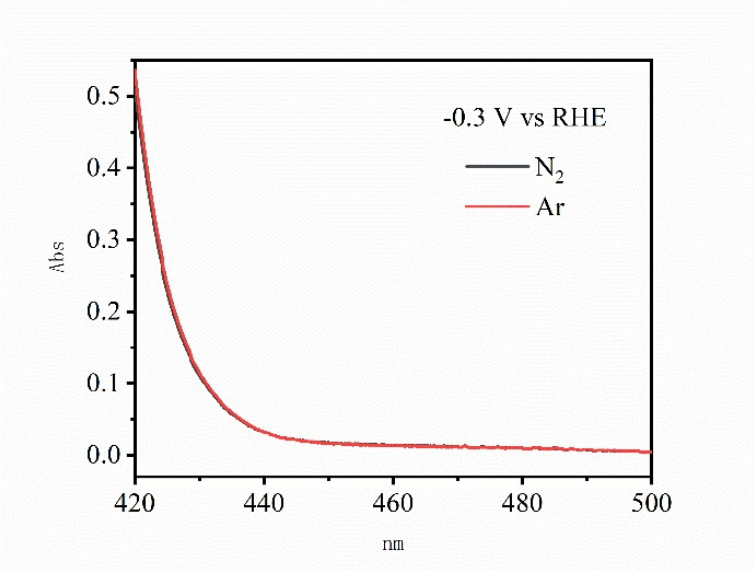

Figure S6. UV-vis absorption spectra by-produced N_2H_4 for AuNFs tested in 0.1 M Li_2SO_4 with bubbled N_2 and Ar under -0.3 V vs. RHE for 2 h.

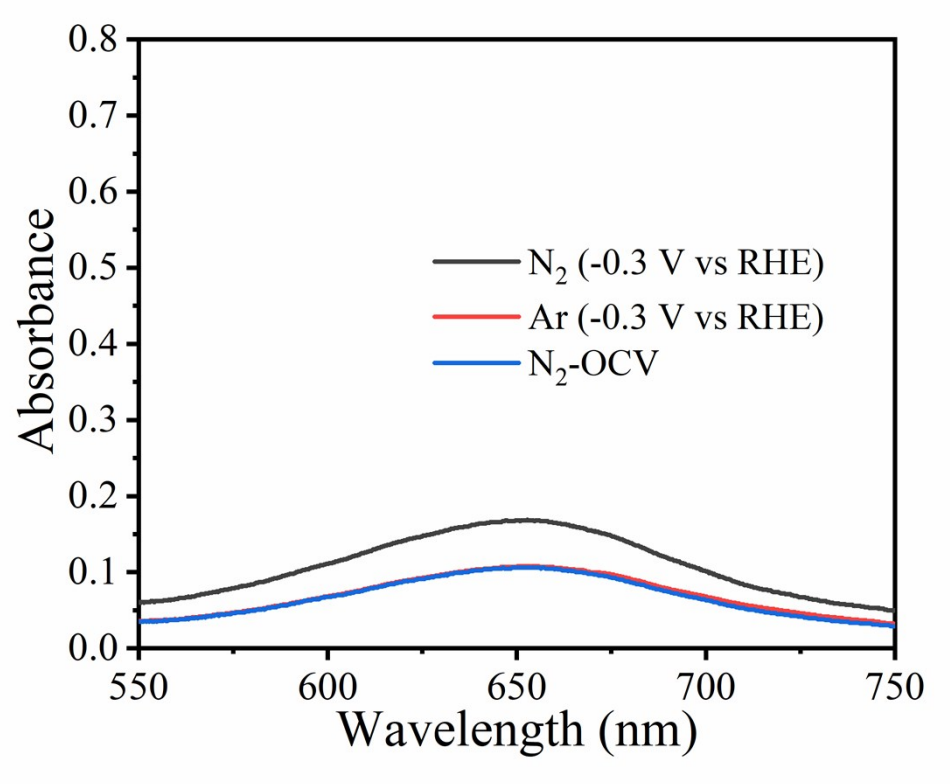

Figure S7. UV-vis absorption spectra of AuNFs in 0.1 M Li_2SO_4 with bubbled N_2 and Ar flow with applied potential (-0.3 V vs. RHE), and continuous N2 flow under open-circuit voltage for 2 h, respectively.

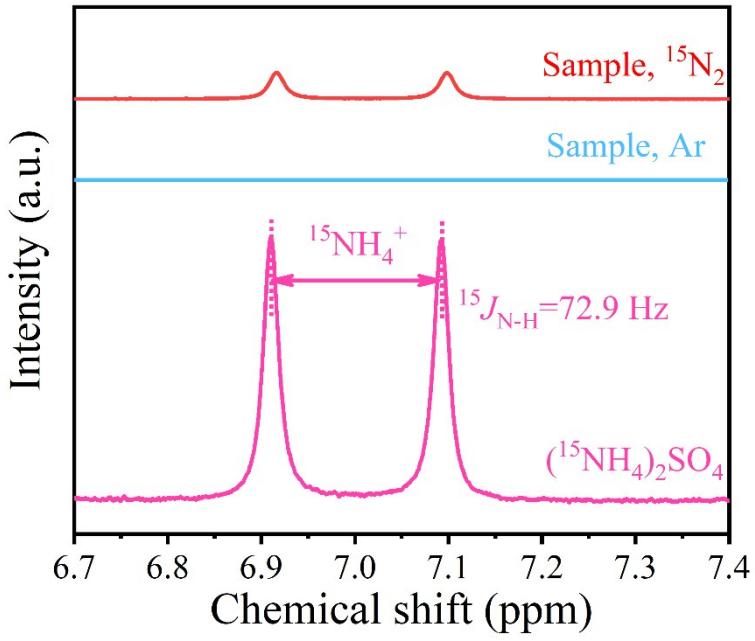

Figure S8. 1H NMR spectra for standard $(^{15}NH_4)_2SO_4$ sample and the electrolytes after electrolysis at -0.3 V vs. RHE using using $^{15}N_2$ and Ar as the feeding gas.

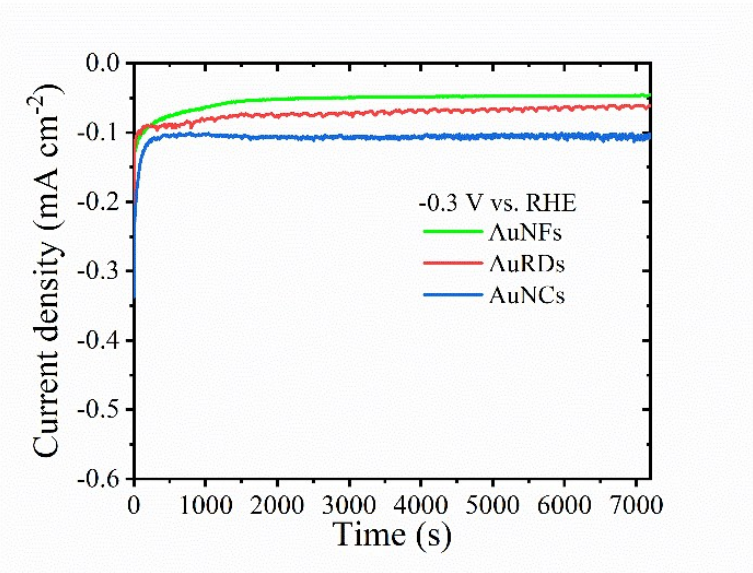

Figure S9. Time-current density curves for AuNFs, AuRDs and AuNCs tested in 0.1 M Li_2SO_4 solution at -0.3 V vs. RHE.

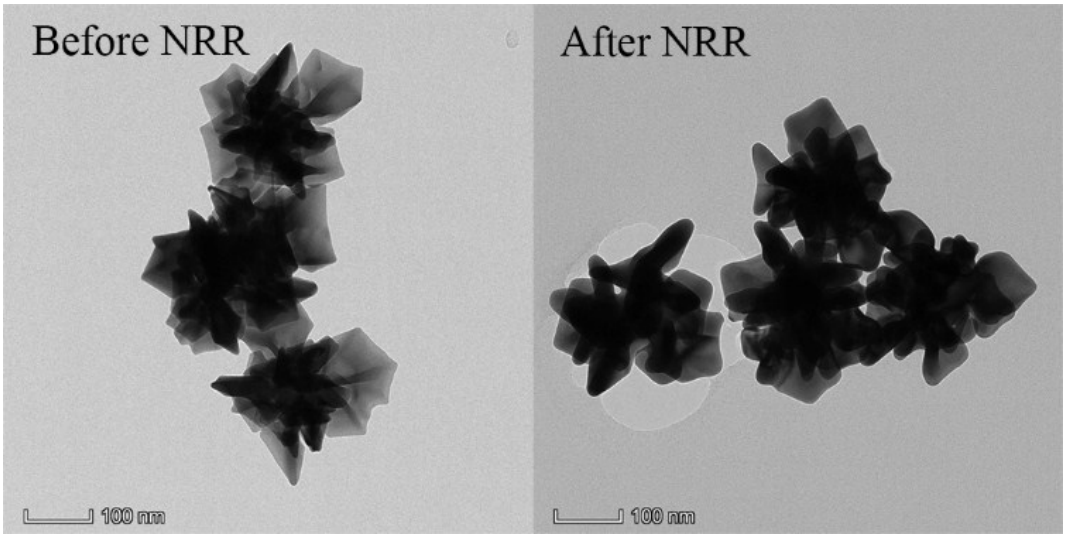

Figure S10. TEM images of AuNFs before and after NRR.

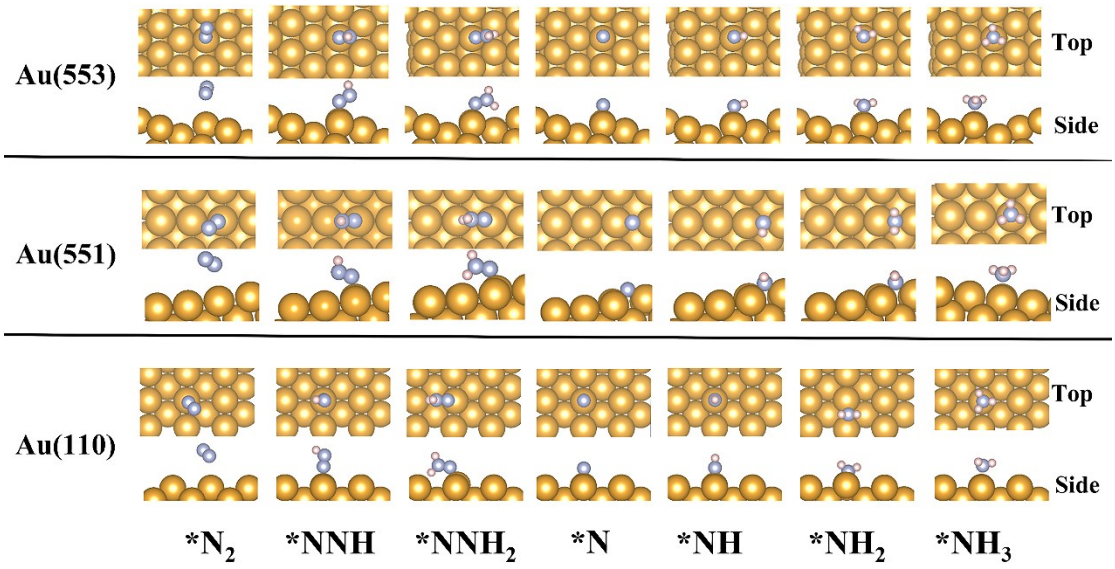

Figure S11. Optimized geometry of reaction intermediates for NRR on Au(553), Au(551) and Au(110), respectively. The orange, steel gray, pale red spheres represent Au, N, and H atoms, respectively.

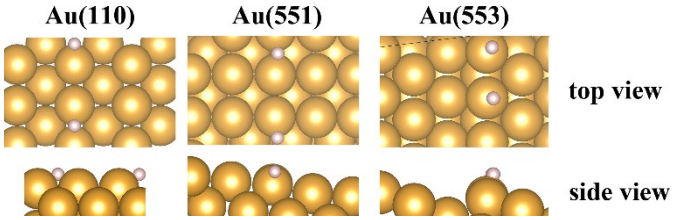

Figure S12. Optimized geometry of 2*H on Au(553), Au(551) and Au(110), respectively. The orange, pale red spheres represent Au and H atoms, respectively.

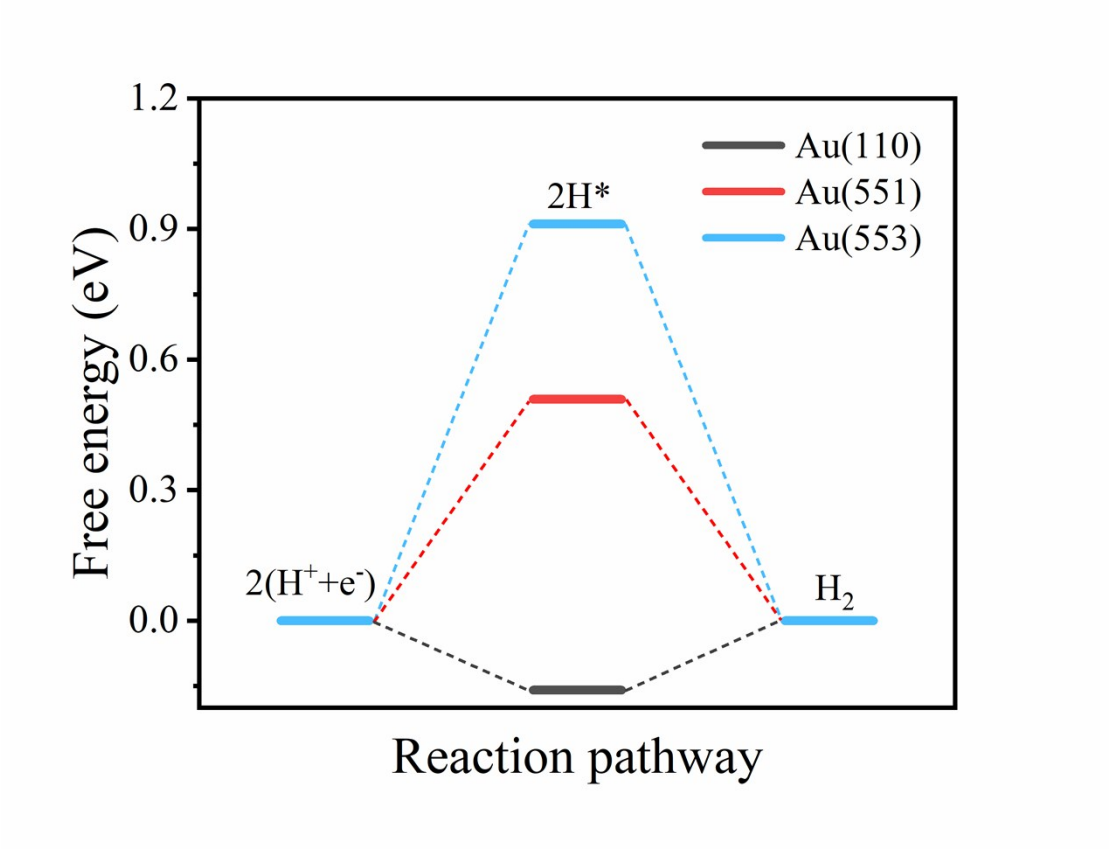

Figure S13 The free energy diagram based on 2*H on Au(110), Au(551) and Au(553), respectively.

Table S1. Comparison of the electrocatalytic NRR performance for AuNPs with other reported catalysts under ambient conditions.

Catalyst	Electrolyte	NH_3 yield rate	FE (%)	Potential (V vs. RHE)	Reference
AuNPs	**0.1 M Li_2SO_4**	**9.22 μg h^{-1} cm^{-2}**	**73.32**	**-0.3**	**This work**
Au nanorod	0.1 M KOH	1.648 μg cm^{-2} h^{-1}	3.88	-0.2	5
AuHNCs	0.5 M $LiClO_4$		35.9	-0.4	6
		3.74 μg cm^{-2} h^{-1}		-0.5	
AuSAs-NDPCs	0.1 M HCl	2.32 μg cm^{-2} h^{-1}	12.3	-0.2	7
Ru@NC	0.1 M HCl	3.66 $mg\ h^{-1} mg_{Ru}^{-1}$		-0.21	8

$Ru@ZrO_2/NC$			21		
RuSAs		120.9 $\mu g_{NH_3} h^{-1} mg_{cat}^{-1}$	29.6	-0.2	9
SA-Mo/NPC	0.1 M KOH	34.0 $\mu g_{NH_3} h^{-1} mg_{cat}^{-1}$	14.6	-0.3	10
NbO_2	0.05 M H_2SO_4	11.6 $\mu g\ h^{-1} mg_{cat}^{-1}$		-0.65	11
			32	-0.6	
Mo_2C nanorod	0.1 M HCl	95.1 $\mu g\ h^{-1}\ mg^{-1}_{cat}$	8.13	-0.3	12
Mn_3O_4 nanocube	0.1 M Na_2SO_4	11.6 $\mu g\ h^{-1}\ mg^{-1}_{cat}$	3	-0.8	13
BC_3	0.05 M H_2SO_4	9.8 $\mu g\ cm^{-2}\ h^{-1}$	10.8	-0.5	14
B_4C nanosheet	0.1 M Na_2SO_4	26.57 $\mu g\ h^{-1}\ mg^{-1}_{cat}$	15.95	-0.75	15
Fe_{SA}-N-C	0.1 M KOH	7.48 $\mu g\ h^{-1}\ mg^{-1}$	56.55	0.193	16
BiNCs	0.5 M K_2SO_4 (pH=3.5)	200 mmol $g^{-1}\ h^{-1}$	66	-0.6	17
MXene/FeOOH	0.01 M HCl		5.78	-0.2	18
		0.53 $\mu g\ cm^{-2}\ h^{-1}$			

Table S2. Calculation results for NRR and HER adsorption on Au(110), Au(551) and Au(553) facets.

All values are in eV.

Facets	ΔG (*H)	ΔG (2*H)	ΔG (*N2)	ΔG (*NNH)	ΔG_{PDS}
Au(110)	-0.23063	-0.15972	0.49541	2.56395	2.06854
Au(551)	0.55030	0.50856	0.49603	2.38173	1.88570
Au(553)	0.48842	0.91119	0.48535	2.32213	1.83678

Reference

1 H.-L. Wu, C.-H. Kuo, and M. H. Huang, *Langmuir* 2010, **26**, 12307-12313.

2 H. E. Lee, K. D. Yang, S. M. Yoon, H. Y. Ahn, Y. Y. Lee, H. Chang, D. H. Jeong, Y. S. Lee,

M. Y. Kim, K. T. Nam, *ACS Nano* 2015, **9**, 8384-8393.
3 D. Zhu, L. H. Zhang, R. E. Ruther, R. J. Hamers, *Nat. Mater.* 2013, **12**, 836–841.
4 G. W. Watt, J. D. Chrisp, *Anal. Chem.* 1952, **24**, 2006-2008.
5 D. Bao, Q. Zhang, F. L. Meng, H. X. Zhong, M. M. Shi, Y. Zhang, J. M. Yan, Q. Jiang, X. B. Zhang, *Adv. Mater.* 2017, **29**, 1604799.
6 M. Nazemi, M. A. El-Sayed, *J. Phys. Chem. Lett.* 2018, **9**, 5160-5166.
7 Q. Qin, T. Heil, M. Antonietti, M. Oschatz, Small Methods 2018, **2**, 1800202.
8 H. C. Tao, C. Choi, L. X. Ding, Z. Jiang, Z. S. Han, M. W. Jia, Q. Fan, Y. N. Gao, H. H. Wang, A. W. Robertson, S. Hong, Y. Jung, S. Z. Liu, Z. Y. Sun, Chem *2019*, **5**, 204-214.
9 Z. G. Geng, Y. Liu, X. D. Kong, P. Li, K. Li, Z. Y. Liu, J. Du, M. Shu, R. Si, J. Zeng, Adv. Mater. *2018*, **30**, 1803498.
10 L. L. Han, X. J. Liu, J. P. Chen, R. Q. Lin, H. X. Liu, F. Lü, S. Bak, Z. X. Liang, S. Z. Zhao, E. Stavitski, J. Luo, R. R. Adzic, H. L. Xin, *Angew. Chem. Int. Ed.* 2019, **58**, 2321-2325.
11 L. S. Huang, J. W. Wu, P. Han, A. M. Al-Enizi, T. M. Almutairi, L. J. Zhang, G. F. Zheng, *Small Methods* 2018, 1800386.
12 X. Ren, J. X. Zhao, Q. Wei, Y. Q. Ma, H. R. Guo, Q. Liu, Y. Wang, G. W. Cui, A. M.A siri, B. H. Li, B. Tang, X. P. Sun, *ACS Cent. Sci.* 2019, **5**, 116-121.
13 X. F. Wu, L. Xia, Y. Wang, W. B. Lu, Q. Liu, X. F. Shi, X. P. Sun, *Small* 2018, **14**, 1803111.
14 X. M. Yu, P. Han, Z. X. Wei, L. S. Huang, Z. X. Gu, S. J. Peng, J. M. Ma, G. F. Zheng, *Joule* 2018, **2**, 1610-1622.
15 W. B. Qiu, X. Y. Xie, J. D. Qiu, W. H. Fang, R. P. Liang, X. Ren, X. Q. Ji, G. W. Cui, A. M. Asiri, G. L. Cui, B. Tang, X. P. Sun, *Nat. Commun.* 2018, **9**, 3485.
16 M. F. Wang, S. S. Liu, T. Qian, J. Liu, J. Q. Zhou, H. Q. Ji, J. Xiong, J. Zhong, C. L. Yan, *Nat. Commun.* 2019, **10**, 341.
17 Y. C. Hao, Y. Guo, L. W. Chen, M. Shu, X. Y. Wang, T. A. Bu, W. Y. Gao, N. Zhang, X. Su, X. Feng, J. W. Zhou, B. Wang, C. W. Hu, A. X. Yin, R. Si, Y. W. Zhang, C. H. Yan, *Nat. Catal.* 2019.
18 Y. R. Luo, G. F. Chen, L. Ding, X. Z. Chen, L. X. Ding, H. H. Wang, *Joule* 2019, **3**, 279-289.
19 M. Bajdich, A. Vojvodic, J. K. Norskov, A. T. Bell, *J. Am. Chem. Soc.* 2013, **135**, 13521-30.